Supporting Information

Pyrolysis of Metal-Organic Frameworks to Hierarchical Porous Cu/Zn-Nanoparticle@Carbon Materials for Efficient CO_2 Hydrogenation

Jingzheng Zhang,[‡a] Bing An,[‡a] Yahui Hong,[a] Yaping Meng,[a] Xuefu Hu,[a] Cheng Wang,*[a] Jingdong Lin,*[a] Wenbin Lin,[ab] Yong Wang[ac]

[a]Collaborative Innovation Center of Chemistry for Energy Materials, State Key Laboratory of Physical Chemistry of Solid Surfaces, Department of Chemistry, College of Chemistry and Chemical Engineering, Xiamen University, Xiamen 361005, People's Republic of China

[b]Department of Chemistry, University of Chicago, 929 East 57th Street, Chicago, Illinois 60637, United States

[c]Voiland School of Chemical Engineering and Bioengineering, Washington State University, Pullman, Washington 99164, United States

[‡] These authors contribute equally

*Corresponding authors: wangchengxmu@xmu.edu.cn; jdlin@xmu.edu.cn.

Table of Contents

S1 General Information

All starting materials were purchased from commercial sources and used without further purification. Copper(II) nitrate hydrate and Zinc nitrate hydrate were purchased from InnoChem Science & Technology (Beijing, China). 1,3,5-benzenetricarboxylic acid (trimesic acid，H_3BTC) were purchased from J&K Scientific (Beijing, China). Activated Carbon were purchased from Energy Chemical (Shanghai, China), N,N-dimethylformamide (DMF) (analytical grade purity) were purchased from Sinopharm Chemical Reagent Co. Ltd.

S2. Details of Synthetic Procedures

Cu-BTC-μm and Zn-Cu-BTC-μm: The MOF precursors were synthesized using a slightly modified literature method.[1] In a typical setup, 3.2 mmol of $Cu(NO_3)_2 \cdot 3H_2O$ (0.76 g) was dissolved in 15 mL of a 1:1 mixture of H_2O and ethanol, and the solution was mixed with 2.0 mmol of trimesic acid (H_3BTC, 0.42 g) in a Teflon vessel placed in an autoclave. The autoclave was heated in an oven at 125 ^oC for 12 h. The blue product was filtered, washed with H_2O and ethanol before drying. Yield: 0.99 g

(75%). Zn-Cu-BTC micron crystals were synthesized in the same way (in 64% yield) except a mixture of $Cu(NO_3)_2 \cdot 3H_2O$ (0.65 g, 2.7 mmol) and $Zn(NO_3)_2 \cdot 6H_2O$ (0.13 g, 0.45 mmol) was used as the metal source. The crystals were collected and used for pyrolysis.

Cu-BTC-submm and Zn-Cu-BTC-submm: The MOF precursors were prepared by a solvothermal reaction based on a modified literature procedure.[2] 1.7 mmol of $Cu(NO_3)_2 \cdot 3H_2O$ (0.41 g) and 0.96 mmol of trimesic acid (H_3BTC, 0.20 g) were reacted in 6 mL of N,N-dimethylformade (DMF) at 90 ^oC for 18 h. Single crystals of Cu-BTC of 0.2-0.4 mm in size were obtained after thorough washing with DMF and ethanol, and sieving between 80 mesh (0.18 mm) and 40 mesh (0.43 mm). Crystal yield: 0.47 g (59%). Zn-Cu-BTC submillimeter crystals were synthesized in the same way (in 53% yield) except that a mixture of $Cu(NO_3)_2 \cdot 3H_2O$ (0.36 g, 1.5 mmol) and $Zn(NO_3)_2 \cdot 6H_2O$ (0.06 g, 0.20 mmol) was used as the metal source. The crystals were collected and used for pyrolysis.

Zn-Cu-BTC-mm: A low temperature solvothermal method was used to synthesize Zn-Cu-BTC-mm crystals based on a slightly modified literature procedure.[3] 1.7 mmol of $Cu(NO_3)_2 \cdot 3H_2O$ (0.42 g) and 0.29 mmol of $Zn(NO_3)_2 \cdot 6H_2O$ (0.086 g) were dissolved in 3 mL of deionized water. 1.1 mmol of H_3BTC (0.24 g) was dissolved in 3 mL of ethanol (slight heating was needed to fully dissolve H_3BTC). The solution of the metallic ions was first mixed with 3 mL of DMF in a 20 mL scintillation vial. The H_3BTC solution and 12 mL of glacial acetic acid (modulator) were subsequently added to the mixed solution. The scintillation vial was placed in an oven at 55 ^oC for 3

days. After filtration and drying, the crystals were collected (50.5% yield) and used for pyrolysis.

Cu-Zn/AC: The AC (Energy Chemical) was pretreated according to literature.[4] 2 M HCl solution was used to purify the commercial AC for 12 h under reflux, then filtered and dried. The AC sample was oxidized with 4 M H_2SO_4 for 4 h. Cu–Zn/AC catalysts were prepared by incipient wetness impregnation. $Cu(NO_3)_2{\cdot}3H_2O$ and $Zn(NO_3)_2{\cdot}6H_2O$ (row ratio = 5:1) were dissolved in deionized water by stirring. Then the mixed metal solution was added to AC suspension under vigorous stirring for 2 h and then aged, centrifuged and dried. After drying, the samples were calcined at 500 ^oC for 2 h under Ar (80mL/min) flow and then activated at 500 ^oC for 2 h under a flow of 5 % H_2/Ar.

Cu-Zn/OMC: The OMC (ordered mesoporous carbon, pore diameter = 3.8-4 nm) was pretreated in the same way as AC, followed by Cu–Zn/OMC prepared by incipient wetness impregnation similar to Cu-Zn/AC (Cu/Zn row ratio = 5:1). After drying, the samples were calcined at 500 ^oC for 2 h under Ar (80 mL/min) flow and then activated at 500 ^oC for 2 h under a flow of 5 % H_2/Ar.

S3. Catalyst Characterization

Thermogravimetric analysis (TGA) was performed in air using a Shimadzu TGA-50 equipped with an Alumina pan. Inductively coupled plasma-optical emission spectrometry (ICP-OES) analyses were performed on an Agilent ICP-OES instrument.

Samples were diluted in 5% HNO_3 matrix and analyzed with a ^{159}Tb internal standard against a six-point standard curve over the range from 1 ppm to 100 ppm. The correlation coefficient was >0.9997 for all analytes of interest. Powder X-ray diffraction (PXRD) was carried out on a Japan Rigaku DMax-γA rotating anode X-ray diffractometer equipped with graphite monochromatized Cu Kα radiation (λ = 1.54 Å). Nitrogen sorption measurements were conducted using a Micromeritics ASAP 3020 system at 77 K. The samples were prepared at 100 °C in vacuum for 5 h. The surface area was calculated using Brunauer-Emmett-Teller (BET) method in the range of P/P_0 = 0.05-0.30. Mesoporous surface areas, pore volumes, and mean pore diameters of mesopores were evaluated by the Barrett-Joyner-Halenda (BJH) method from the adsorption branches of isotherms. Transmission electron microscopy (TEM) and EDX mapping were performed on JEOL 1400 and Phillips Analytical FEI Tecnai F30 electron microscope operated at an electron acceleration voltage of 300 kV. Scanning electron microscope (SEM) studies were performed on ZEISS SIGMA. X-ray photoelectron spectroscopy (XPS) measurements were carried out with a Qtac-100 LEISS-XPS spectrometer with a hemispherical electron energy analyzer and a home-made reaction chamber. Monochromatic Al Kα X-ray source (1486.6 eV, anode operating at 300 W) was used as the excitation source. The energy analysis error of the measurement was ± 0.2 eV for binding energy.

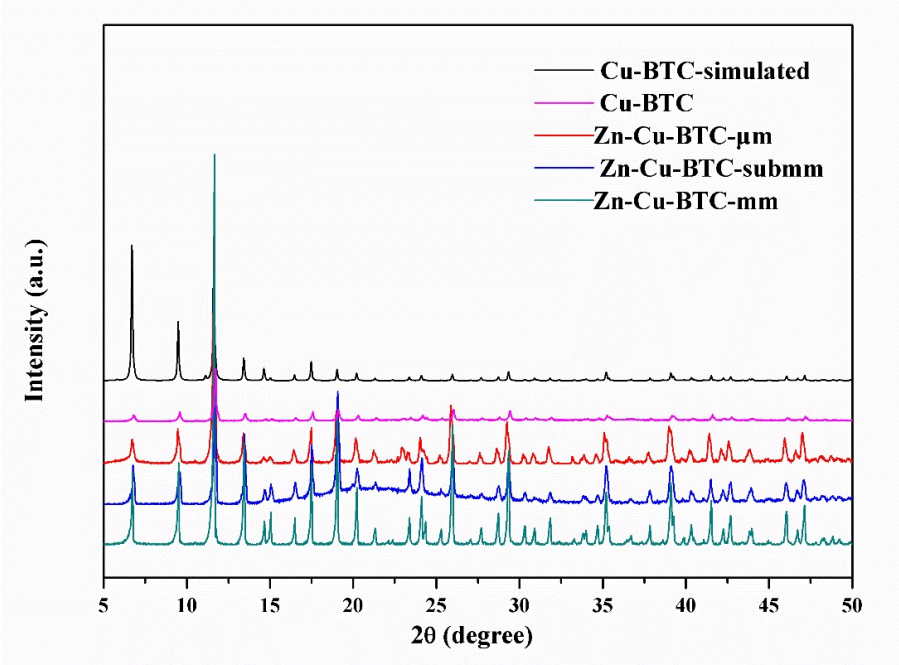

Figure S1. PXRD of Cu-BTC and Zn-Cu-BTC crystals with different sizes.

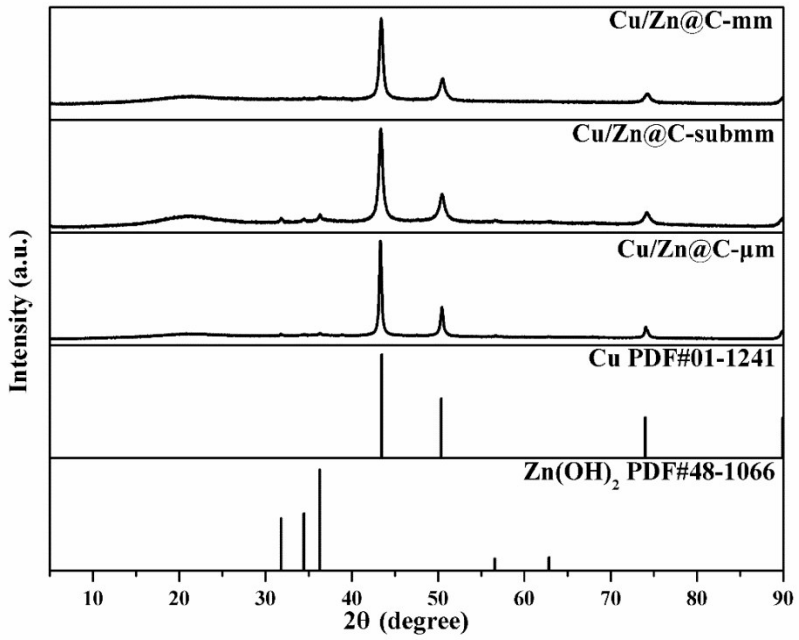

Figure S2. PXRD patterns of MOF-derived Cu/Zn@C materials, Cu, and $Zn(OH)_2$.

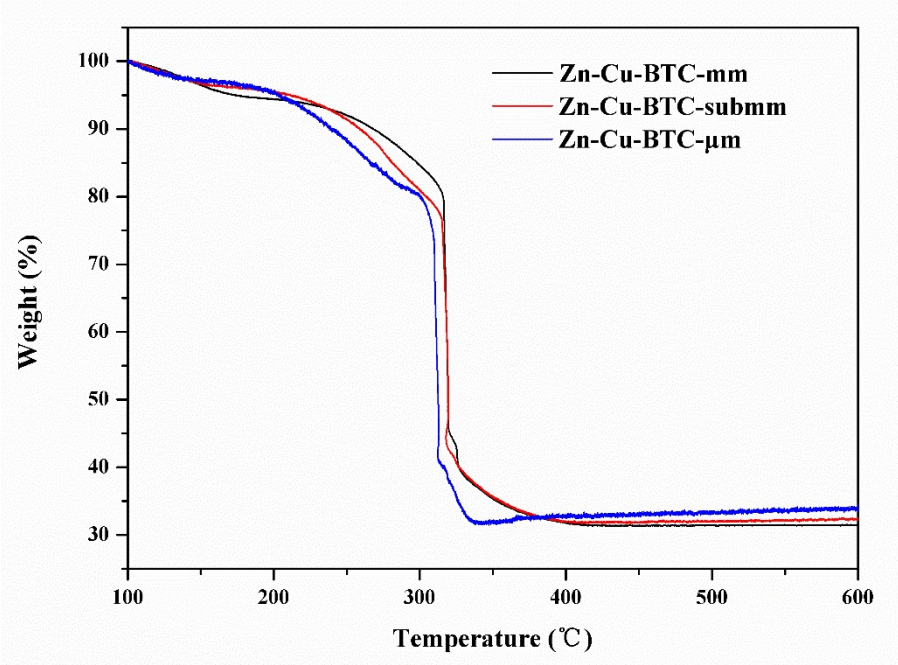

Figure S3. TGA curve of Zn-Cu-BTC with different particle sizes in the 100-600 ^{o}C range. Conditions: air atmosphere (20 mL min^{-1}), heating rate 5 ^{o}C min^{-1}.

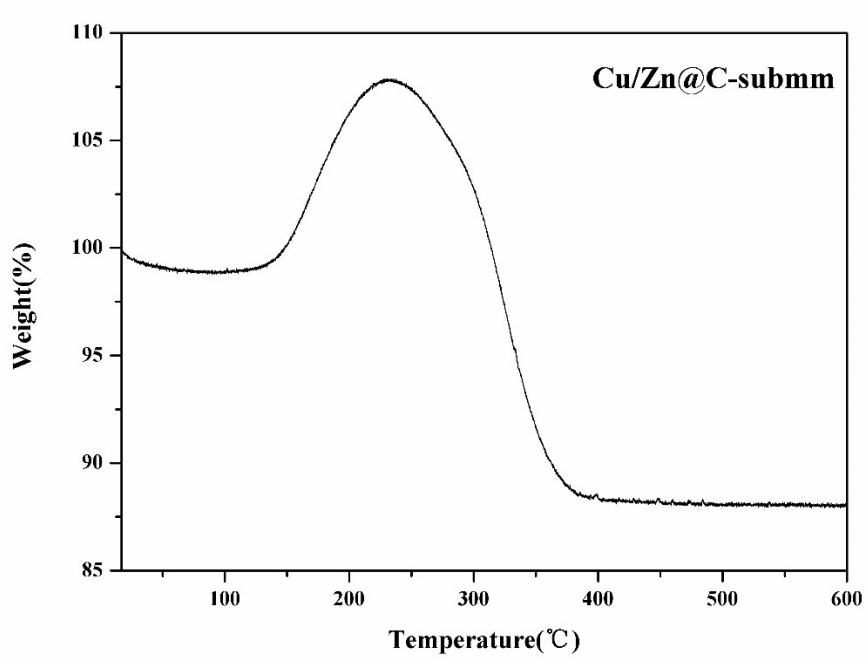

Figure S4. TGA curve of Cu/Zn@C-submm in the 20-600 ^{o}C range. Conditions: air atmosphere (20 mL min^{-1}), heating rate 5 ^{o}C min^{-1}. The mass increase between 150-250 ^{o}C was due to the oxidation of metallic Cu to copper oxide. The weight percentage of Cu/Zn is about 70 wt% as derived from the residual mass of CuO/ZnO

(88.1 wt%).

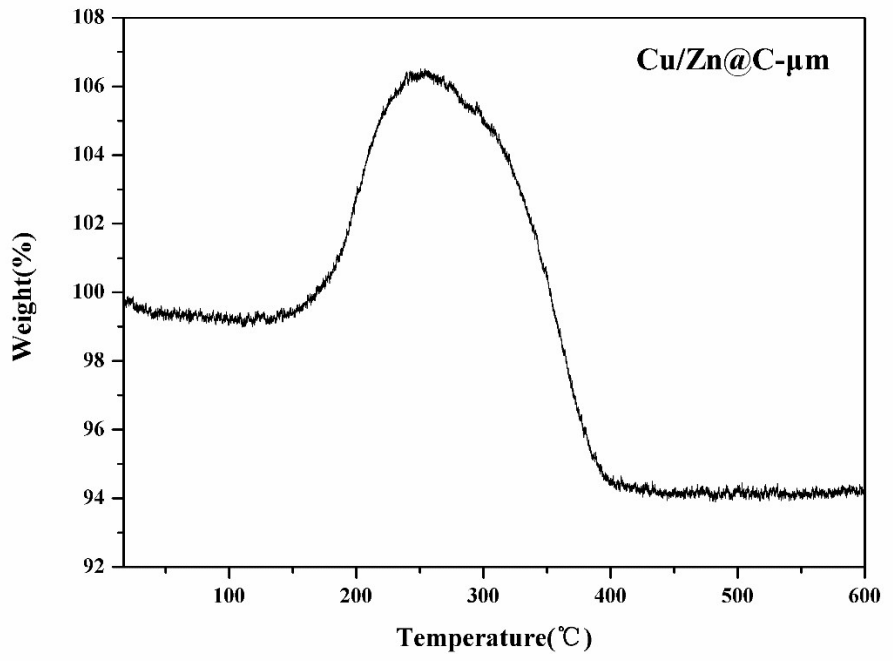

Figure S5. TGA of Cu/Zn@C-µm in the 20-600 °C range. Conditions: air atmosphere (20 mL min^{-1}), heating rate 5 °C min^{-1}. The mass increase between 150-250 °C was due to the oxidation of metallic Cu to copper oxide. The weight percentage of Cu/Zn is about 75 wt% as derived from the residual mass of CuO/ZnO (94.1 wt%).

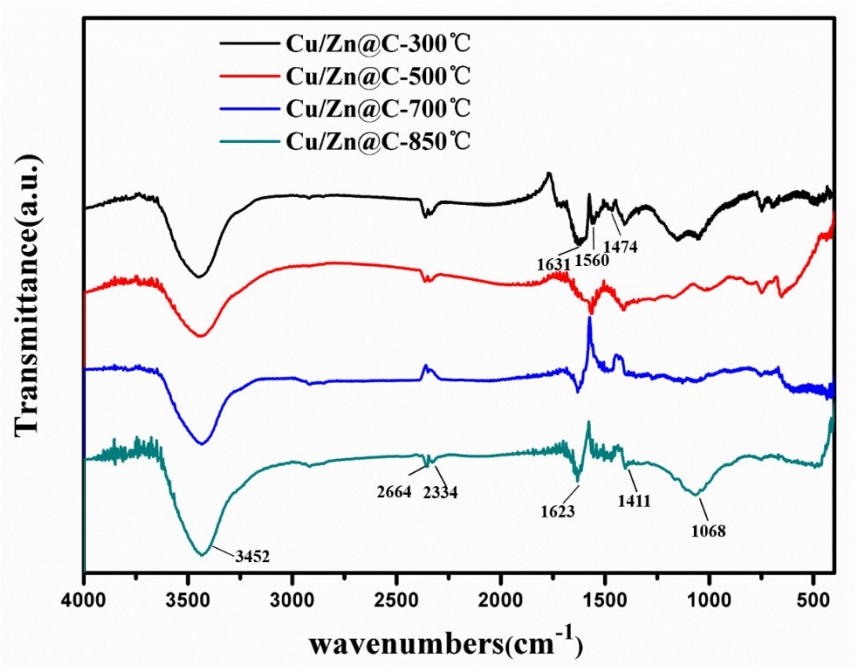

Figure S6. FTIR spectrum of Cu/Zn@C materials obtained by pyrolyzing at different

temperatures. Pyrolysis condition: argon flow of 80 mL min^{-1}, the same temperature program as in pyrolysis procedure described in the main article, except for the target temperature of 300 °C, 500 °C, 700 °C and 850 °C. Cu/Zn@C-300 °C has absorption peaks corresponding to benzene ring vibrations at 1631 cm^{-1}, 1560 cm^{-1} and 1474 cm^{-1}, while these features were lost in samples pyrolyzed above 500 °C. These results suggest that the benzene rings were fully converted carbon materials at these temperatures. Furthermore, the absorption peaks at 1623 cm^{-1} and 1068 cm^{-1} can be assigned to C=O stretching and C-C stretching, respectively, while the 1411 cm^{-1} peak is attributed to OH bending.

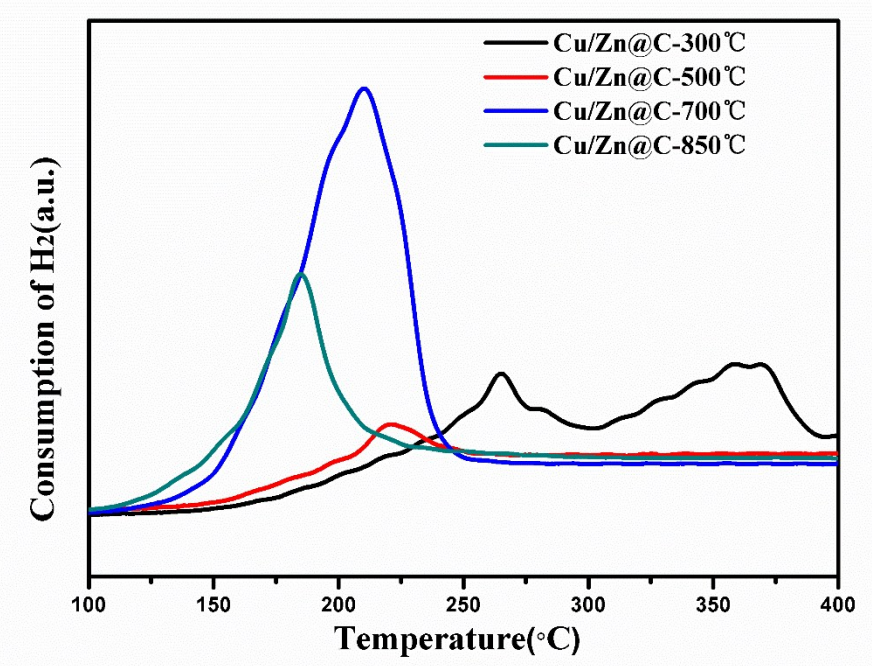

Figure S7. H_2-TPR of Cu/Zn@C materials. Within the temperature range of 100-400 °C, there was only one reduction peak for Cu/Zn@C-500 °C, Cu/Zn@C-700 °C, and Cu/Zn@C-850 °C catalysts, implying a single reduction step of Cu_2O ($Cu^{+}\rightarrow Cu^{0}$).[5] The presence of more than one reduction peak for Cu/Zn@C-300 °C suggests stepwise reduction ($Cu^{2+}\rightarrow Cu^{+}\rightarrow Cu^{0}$) for this sample.[6]

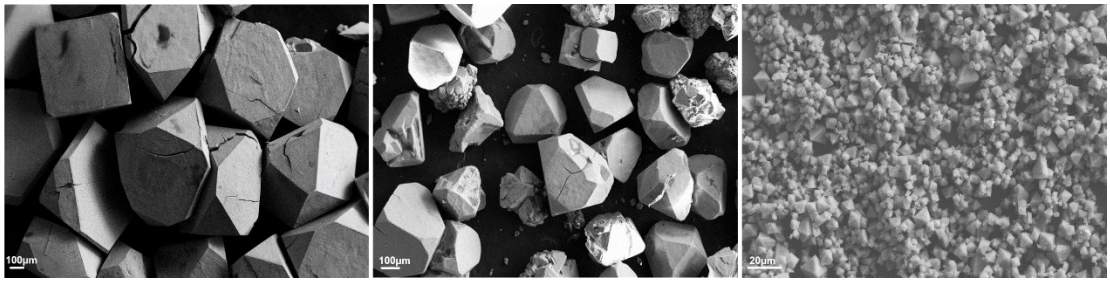

Figure S8. SEM images of Cu/Zn@C materials with different particle sizes. From left to right: Cu/Zn@C-mm, Cu/Zn@C-submm, and Cu/Zn@C-μm.

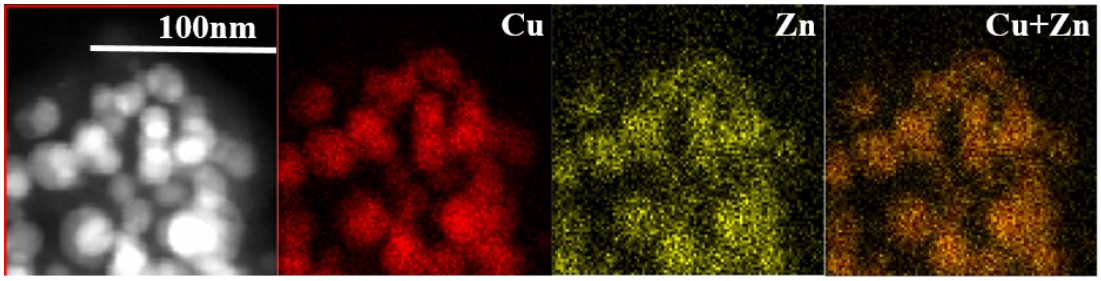

Figure S9. EDX mapping of Cu/Zn@C-submm after reaction, showing well mixed Cu and Zn.

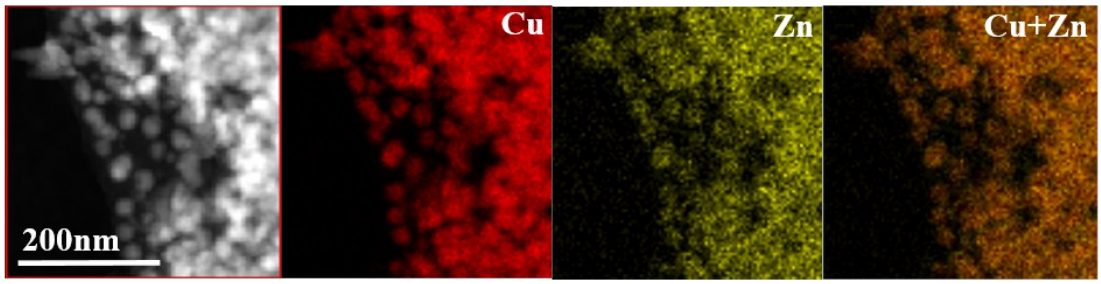

Figure S10. EDX mapping of Cu/Zn@C-μm.

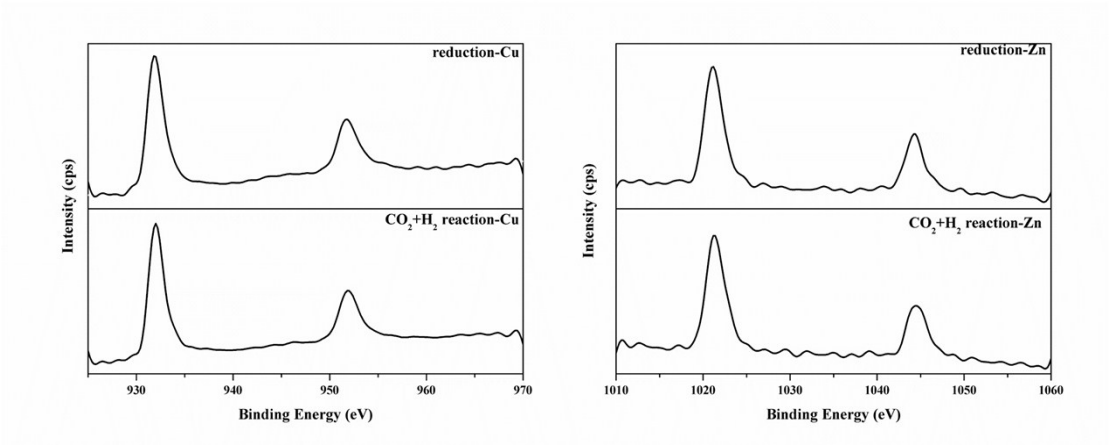

Figure S11. XPS of Cu/Zn@C-submm after reduction and treatment with reaction gas. In XPS analysis, the sample was reduced with 5% H_2 in Ar at 250 ^oC for 1 h or followed by reaction gas treatment for 3 h. The XPS spectra showed peaks at 951.8 eV and 931.8 eV for Cu $2p_{1/2}$ and $2p_{3/2}$, respectively, both after H_2 gas and reaction gas treatment. This result suggests that copper is in 0 valence state under these conditions. On the other hand, the peaks at 1021.2 eV and 1044.5 eV are consistent with the $2p_{3/2}$ and $2p_{1/2}$ transitions of Zn(Ⅱ), respectively.

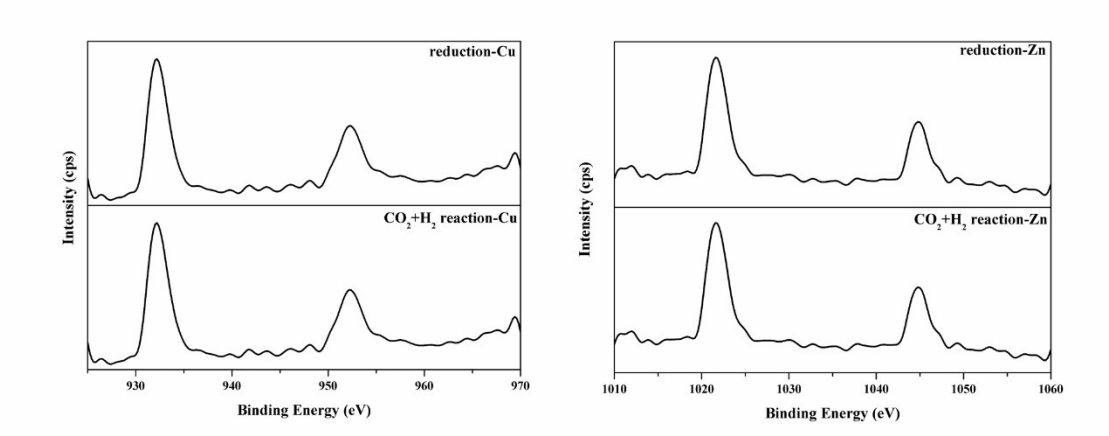

Figure S12. XPS of Cu/Zn@C-μm after reduction and treatment with reaction gas.

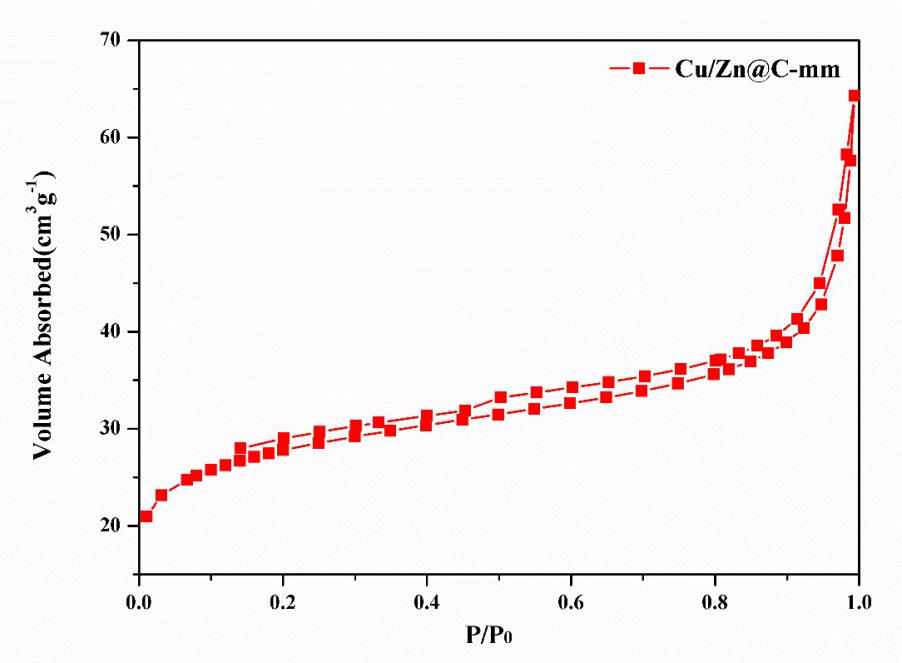

Figure S13. N_2 sorption isotherms of Cu/Zn@C-mm at 77 K.

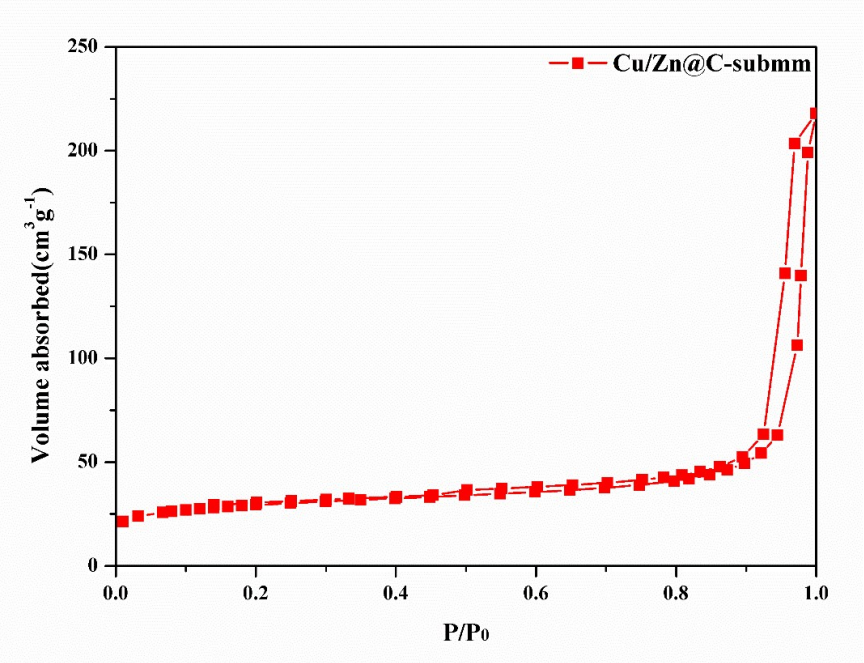

Figure S14. N_2 sorption isotherms of Cu/Zn@C-submm at 77 K.

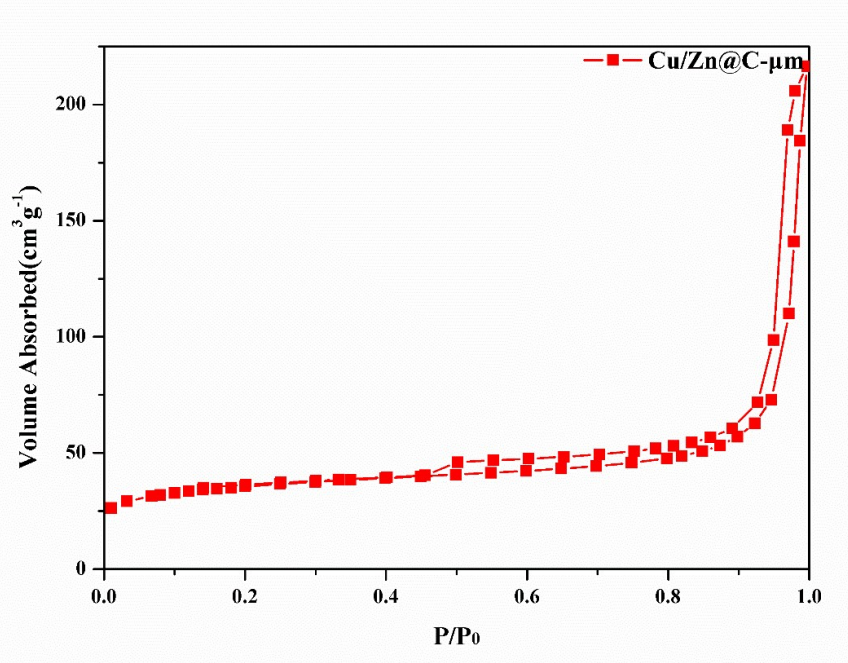

Figure S15. N_2 sorption isotherms of Cu/Zn@C-μm at 77 K.

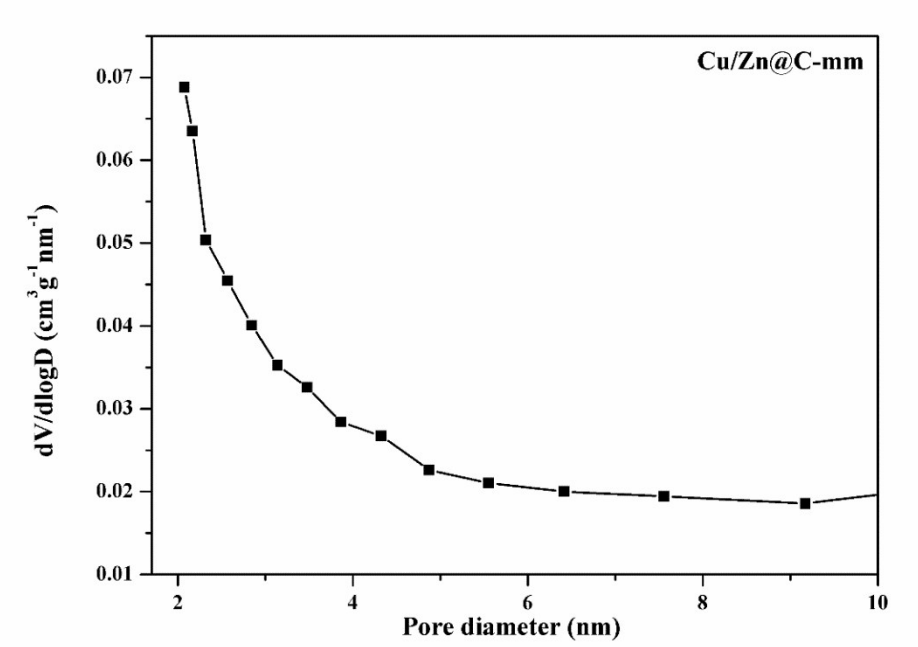

Figure S16. The pore size distribution of Cu/Zn@C-mm. The pore size distribution curves were calculated by the BJH method.

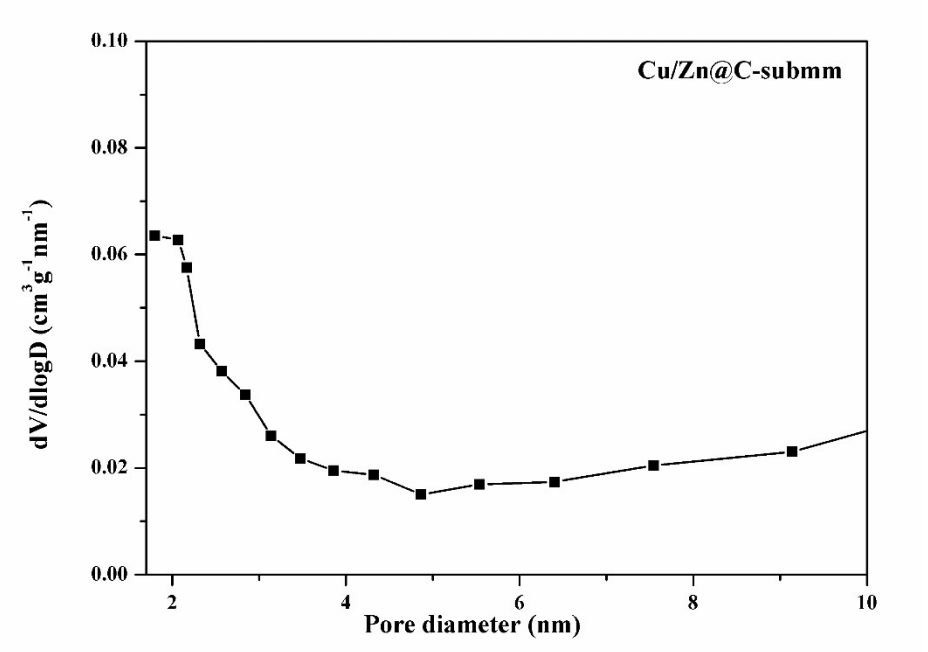

Figure S17. The pore size distribution of Cu/Zn@C-submm. The pore size distribution curves were calculated by the BJH method.

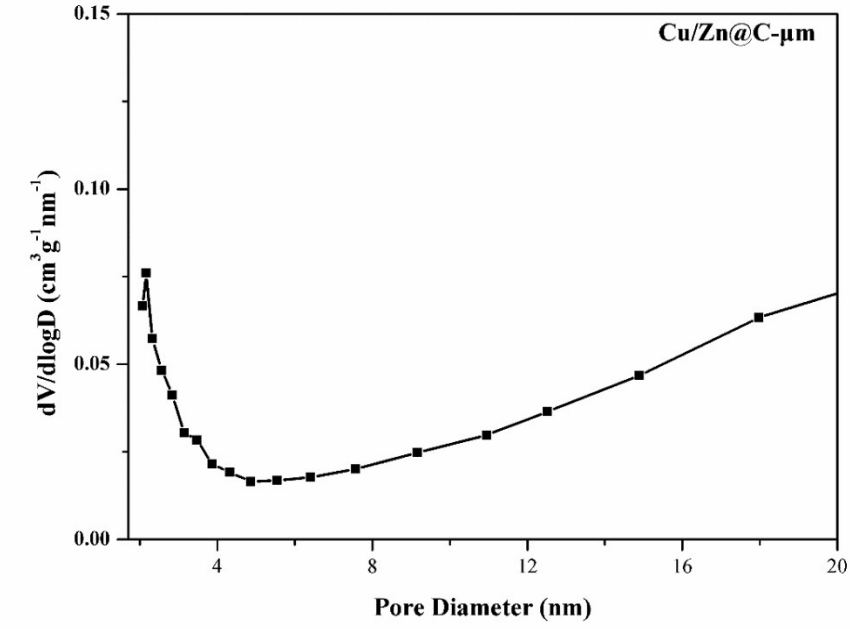

Figure S18. The pore size distribution of Cu/Zn@C-μm. The pore size distribution curves were calculated by the BJH method.

Table S1. Elemental analysis, ICP-OES, and N_2 sorption results of the MOF-derived Cu/Zn@C materials.

Catalyst	Element content (wt%)			Pore width (nm)	S_{BET} (m^2g^{-1})
	Cu[a]	Zn[a]	C[b]		
Cu/Zn@C-submm	67.2	3.4	11.9	6.5	125.03
Cu/Zn@C-μm	73.7	2.1	5.3	5.5	123.09
Cu/Zn@C-mm	69.0	2.8	10.3	3.1	95.85

[a] Determined by ICP-OES.

[b] Determined by Elemental Analysis.

N_2O treatment is a process of dissociative N_2O adsorption followed by H_2 titration. The experiment was carried out on a Micromeritics AutoChem 2920 instrument. The catalyst (100 mg) was placed in a tube reactor and was first reduced in a mixture of 5% H_2-Ar (30 mL min^{-1}) for 2 h at 250 °C with a programmed temperature ramp of 10 °C/min. Then, the reduced samples were cooled to 50 °C and isothermally purged with Ar for 15 min, after which the sample was exposed to N_2O (50 mL min^{-1}) for 30 min to ensure complete oxidation of surface Cu. The samples were then flushed with Ar to remove the excess N_2O. Finally, a pulse of 5% H_2-Ar was passed over the catalyst at 400 °C, and the consumption of H_2 was quantified by the thermal conductivity detector. The reaction sequence is:

$$2\mathrm{Cu} + N_2O \longrightarrow Cu_2O + N_2$$
$$Cu_2O + H_2 \longrightarrow 2Cu + H_2O$$

It is also possible that ZnO can be partially reduced by H_2. However, we did not observe significant H_2 consumption in the second step. As H_2 consumption can be observed in independent TPR experiment, we concluded that Cu surface was not oxidized by N_2O in these experiments at 50 ^oC, especially for Cu particle sizes larger than 20nm. A higher temperature is expected to readily oxidize not only the Cu surface but also bulk Cu. This resistance to oxidation is consistent with the observation of metallic Cu in the sample by PXRD even after leaving the sample in air for one month.

S4. Catalytic Test

100 mg of the catalyst was loaded into the reaction tube (9mm) sandwiched between two layers of glass wools (bed height is 4-6 mm). The catalysis was carried out with a mixture gas of H_2/CO_2 = 3/1 (with 5% of Ar as internal standard) with a total pressure of 1 bar at 300 ^oC and a flow rate of 30 mL/min. The reaction was kept on stream for 20 h, and the reaction mixture was regularly sampled by an automatic online gas chromatography analysis system to determine the conversion and selectivity. The amounts of CO_2 and CO in the flow were quantified by a thermal conductivity detector (TCD) and the amounts of methanol and methane were quantified by a flame ionization detector (FID).

Table S2. Comparisons of the Catalytic Performances

Entry	Catalyst	H_2:CO_2 ratio	Temp. (°C)	P (bar)	CO_2 Conv.%[a]	Select.%[a]			Ref
						CO	CH_3OH	CH_4	
1	Cu/Zn@C-submm	3:1	500	1	5.0	100	0	0	This work
2		3:1	300	1	7.5	11.3	0.8	87.9	This work
3		3:1	300	40	17.0	88.5	11.5	0	This work
4		3:1	260	40	12.8	58.3	41.7	0	This work
5	Cu@C-submm	3:1	500	1	1.9	90.4	0	9.6	This work
6		3:1	300	1	2.1	25.7	0.3	74.0	This work
7		3:1	300	40	5.6	99.4	0.2	0.4	This work
8		3:1	260	40	2.0	41.7	58.3	0	This work
9	Cu-Zn-Al	2:1	500	1	N/A	100	0	0	[7]
10	Cu/SiO_2	1:1	500	1	1.8	N/A	N/A	N/A	[8]
11	$Cu/\beta\text{-}Mo_2C$	2:1	300	1	N/A	96.5	N/A	N/A	[7]
12	$PtCo/\gamma\text{-}Al_2O_3$	3:1	300	1	5.1	89.4	N/A	N/A	[9]
13	$Co/\gamma\text{-}Al_2O_3$	3:1	300	1	3.8	67.0	N/A	N/A	[9]
14	Li/RhY	3:1	250	30	13.1	86.6	N/A	N/A	[10]
15	Au/ZnO	3:1	240	50	1.0	30	70	0	[11]

[a] The conversions and selectivities are the average values over reactions of 20 h.

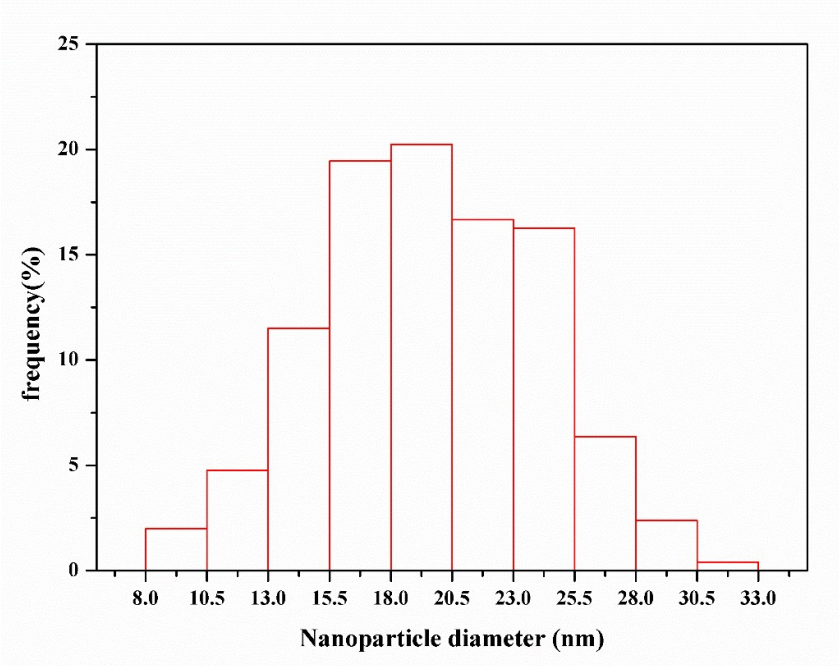

Figure S19. Size distribution of NPs in Cu/Zn@C-submm.

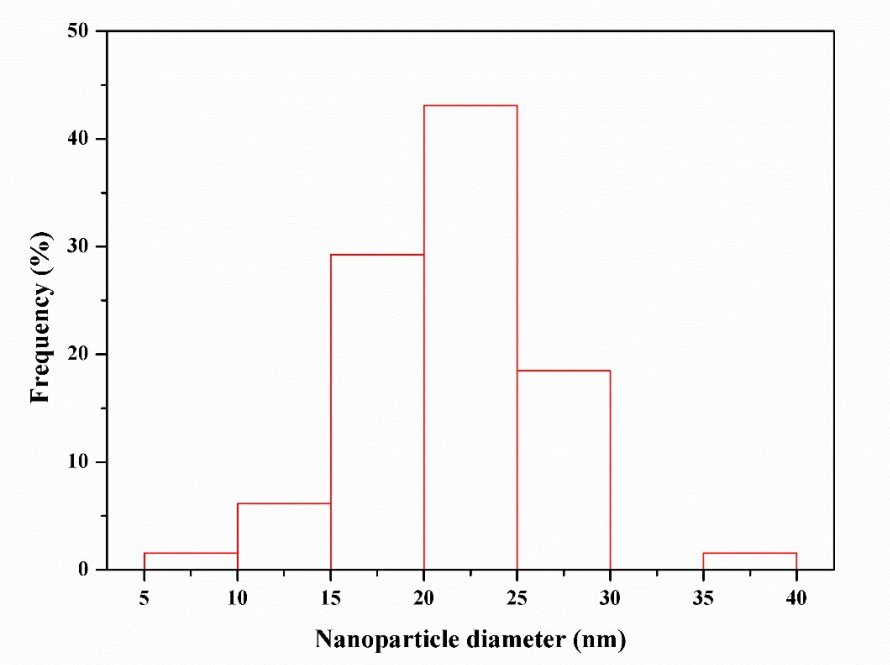

Figure S20. Size distribution of NPs in Cu/Zn@C-submm after reaction at 300°C and 40 bar (H_2/CO_2 = 3/1) for 20 h.

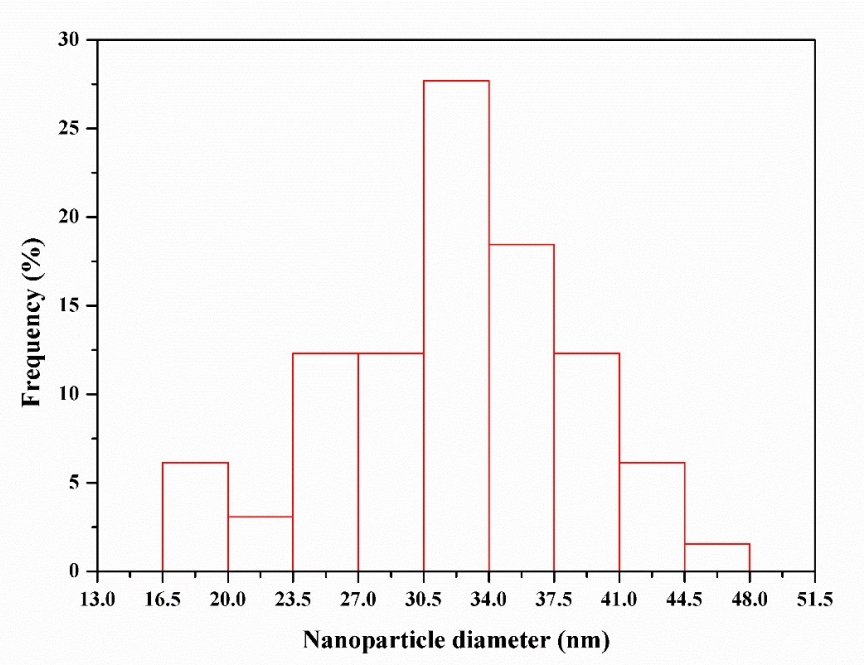

Figure S21. Size distribution of NPs in Cu/Zn@C-submm after reaction at 500 °C and 1 bar (H_2/CO_2 = 3/1) for 20 h.

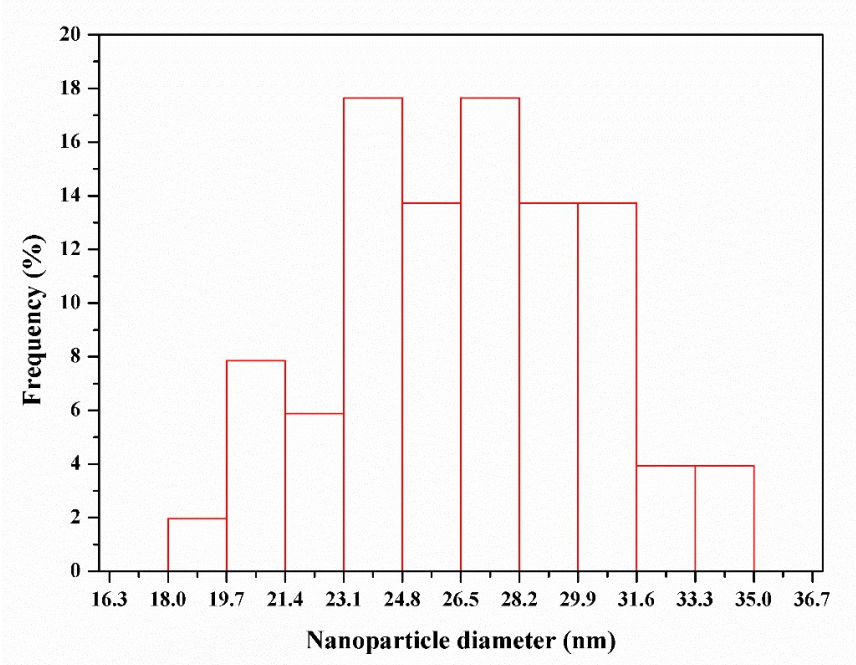

Figure S22. Size distribution of NPs in Cu/Zn@C-μm.

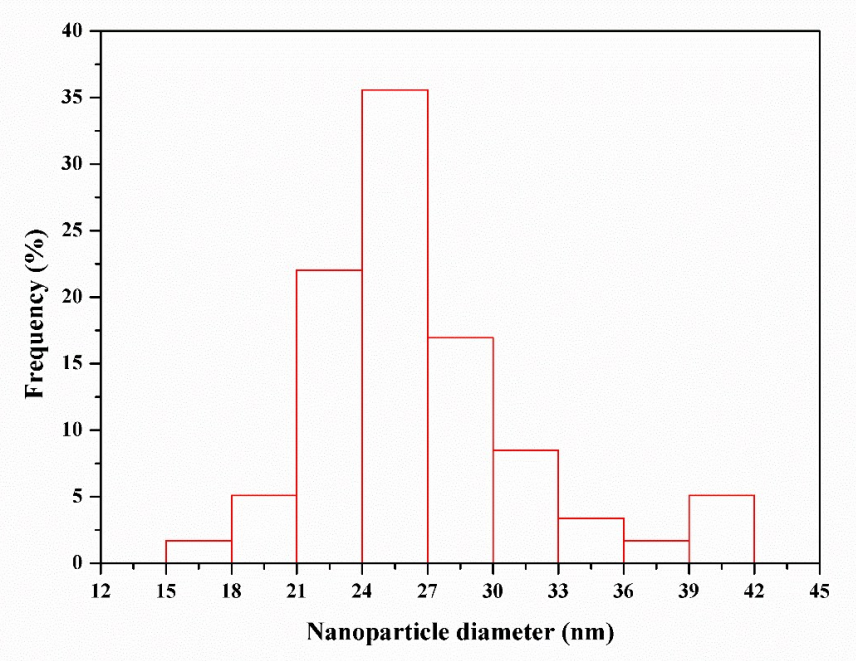

Figure S23. Size distribution of NPs in Cu/Zn@C-μm after reaction at 300 °C and 40 bar (H_2/CO_2 = 3/1) for 20 h.

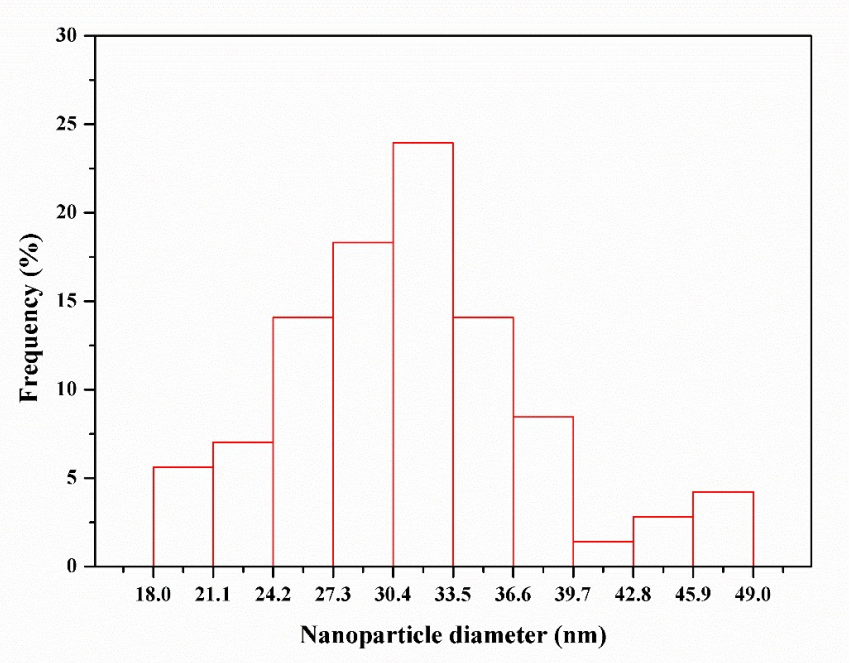

Figure S24. Size distribution of NPs in Cu/Zn@C-µm after reaction at 500 °C and 1 bar (H_2/CO_2 = 3/1) for 20 h.

Table S3. Catalyst nanoparticle size before and after reaction.

Catalyst	before reaction (nm)	300°C-after reaction[a] (nm)	500°C-after reaction[b] (nm)
Cu/Zn@C-submm	20 ± 5	22 ± 4	31 ± 8
Cu/Zn@C-µm	27 ± 4	27 ± 4	31 ± 4

[a] H_2/CO_2 = 3/1, P = 40 bar, GHSV = 18000 h^{-1}

[b] H_2/CO_2 = 3/1, P = 1 bar, GHSV = 18000 h^{-1}

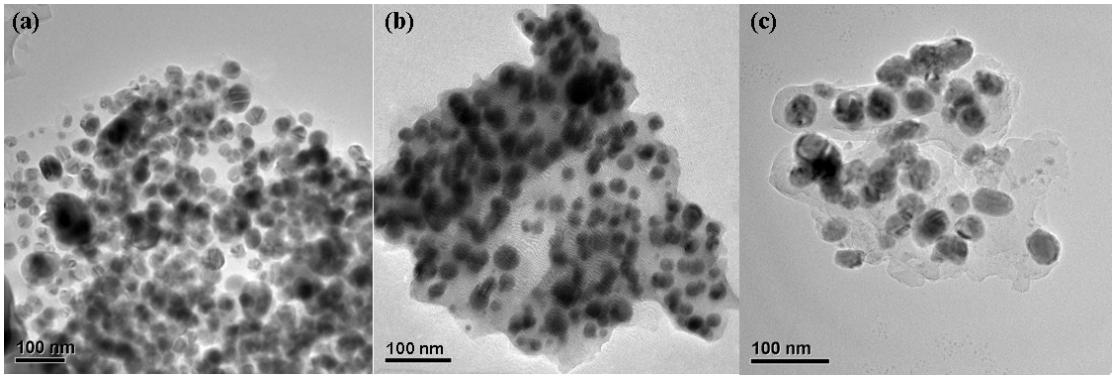

Figure S25. (a) TEM images of Cu/Zn@C-μm after reaction at 300 °C and 40 bar; TEM images of pieces striped from (b) Cu/Zn@C-submm (c) Cu/Zn@C-mm after reaction at 300 °C and 40 bar.

After reaction at 300 °C and a higher pressure of 40 bar, no statistically significant changes of the size and shape of the embedded NPs were observed (Figure S21b and Table S3, 20 ± 5 nm before reaction vs. 22 ± 4 nm after reaction).

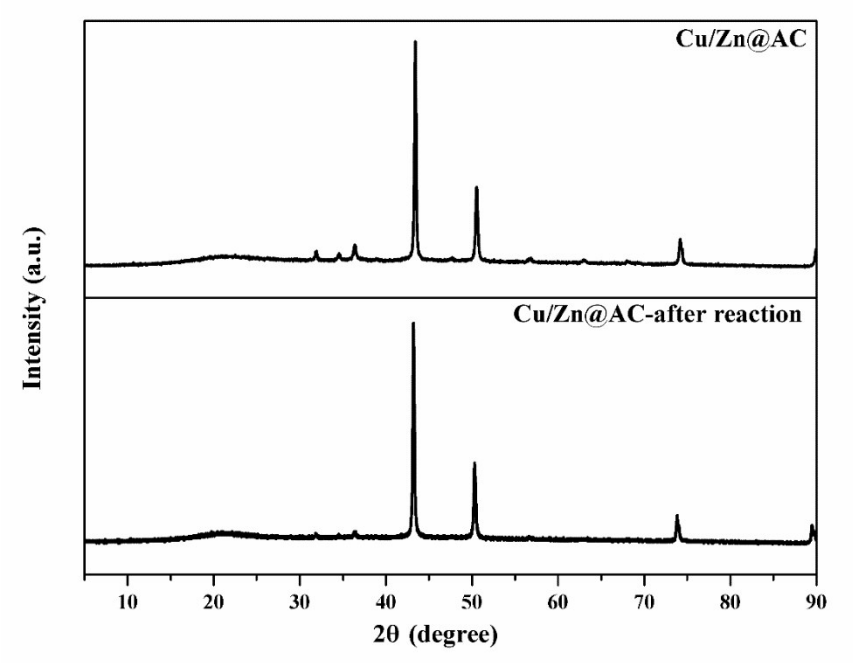

Figure S26. PXRD patterns of Cu-Zn/AC before reaction and after reaction at 500 °C and 1 bar.

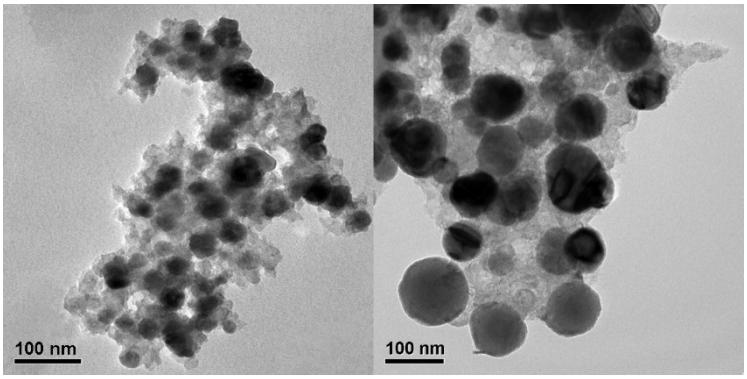

Figure S27. (a) TEM images of Cu-Zn/AC before reaction; (b) Cu-Zn/AC after reaction at 500 ^{o}C and 1 bar. Obvious nanoparticle aggregation was observed for these catalysts.

S5. Effects of Pellet Size

Table S4. Pressure drops for catalysts with different particle sizes

Catalyst	Bed height (mm)	Pressure drop (Pa)
Cu/Zn@C-μm	7.5	1270
Cu/Zn@C-submm	6	100
Cu/Zn@C-mm	4.5	60

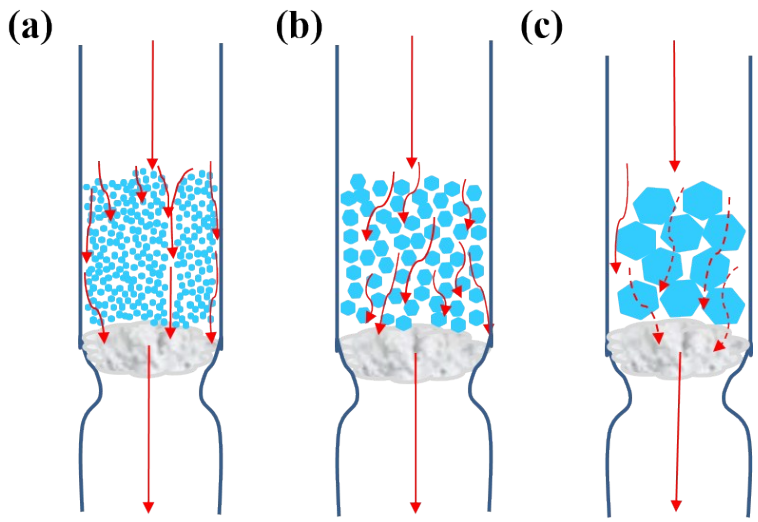

Scheme S1. Different flow modes for catalysts with different sizes. (a) Cu/Zn@C-μm (b) Cu/Zn@C-submm (c) Cu/Zn@C-mm.

We also quantified the pressure drops in the reaction beds of catalysts with different pellet sizes. 50 mg of Cu/Zn@C-submm, Cu/Zn@C-μm and Cu/Zn@C-mm were put into a quartz tube under a flow of Ar (30mL/min) to simulate the flow under reaction condition. The pressure differences before and after the catalyst beds were measured by a differential gauge and were shown in Table S4. Cu/Zn@C-μm showed an obvious pressure drop of 1270 Pa, while the Cu/Zn@C-submm and Cu/Zn@C-mm only showed pressure drops of 100 Pa and 60 Pa respectively. The catalysts with small pellet sizes thus exhibit a much higher pressure drop in the bed. The bed heights of the three catalysts are also different as the fill factors of catalysts of different pellet sizes follow the order Cu/Zn@C-mm > Cu/Zn@C-submm > Cu/Zn@C-μm.

Table S5. Performances of Cu/Zn@C catalysts with different pellet sizes

Catalyst	T = 260 °C P = 40 bar[a]	T = 300 °C P = 1 bar	T = 500 °C P = 1 bar

Cu/Zn@C-μm	7.2%	0.1%	0.7%
Cu/Zn@C-submm	12.8%	7.5%	5.0%
Cu/Zn@C-mm	5.3%	1.3%	4.1%

[a] H_2/CO_2 = 3/1, GHSV = 18000 h^{-1}.

As shown in Table S5, we examined the activities of the catalysts pyrolyzed from MOF crystals of different sizes (Cu/Zn@C-μm, Cu/Zn@C-submm and Cu/Zn@C-mm). Both Cu/Zn@C-μm and Cu/Zn@C-mm showed much lower catalytic activities than that of Cu/Zn@C-submm. For example, at 500 ^oC and 1 bar, the Cu/Zn@C-μm gave a CO_2 conversion of only 0.7% as compared to 5.0% for Cu/Zn@C-submm. At 300 ^oC and 1 bar, the Cu/Zn@C-μm also gave a low CO_2 conversion of 0.1% as compared to 7.5% for Cu/Zn@C-submm. At a higher pressure of 40 bar and 260 ^oC, the conversion of Cu/Zn@C-μm increased to 7.2%, but was still significantly lower than 12.8% for Cu/Zn@C-submm under the same condition.

To explore the factors responsible for the drastically different activities between Cu/Zn@C-submm and Cu/Zn@C-μm**,** we compared the sizes of Cu/Zn NPs in these two catalysts (20 ± 5 nm vs. 27 ± 4 nm, Table S3), the BET surface areas and pore size distributions of the carbon matrixes in the two catalysts (125.03 m^2/g vs. 123.09 m^2/g, see Table S1 and Figures S9-S14) and the Zn doping levels in the two samples (3.4% vs. 2.1%, Table S1). None of these factors showed significant differences to account for the difference in activities. We thus attribute this activity difference to the different pellet sizes.

It is established that an optimum pellet size of a supported catalyst is usually 1/50-1/100 of the bed height, or 1/6-1/10 of the diameter of the reaction tube (when bed height/diameter > 6) for a fixed bed reactor. When the pellet size is too small, a high pressure drop is built around the catalyst bed to increase the chance of channeling, in which the gas flow drills holes on the catalyst bed and short-circuits through without contacting with the catalyst. Furthermore, the small pellet of microns in size also gives inter-pellet channels of microns in size that leads to a small Reynold's number and laminar flow in the reaction bed, while turbulent flow is preferred to bring all reaction gases into contact with the catalyst pellet. Both of these factors pass the reaction gas away from the catalysts and deleteriously affect the conversion. As the activity reduction in Cu/Zn@C-μm is more pronounced at lower pressure (1 bar) that produces smaller Reynold's number, the laminar flow in narrow inter-pellet space might be the primary reason for the low activities of Cu/Zn@C-μm.

An alternative explanation is that CO_2 RWGS has non-zero order kinetics with respect to CO_2 and H_2 partial pressures. A pressure drop in the column with Cu/Zn@C-μm catalyst causes a dramatic effect on the kinetics. This pressure drop had a less effect at 40 bar as compared to 1 bar.

On the other hand, when the pellets are too large, intra-pellet diffusion becomes a significant resistance to mass transport, rendering a large portion of the catalysts unused and leading to decreased activity. This notion is consistent with the much lower CO_2 conversion of Cu/Zn@C-mm than that of Cu/Zn@C-submm at low

temperatures (5.3% vs. 12.8% at 260 °C, 40 bar and 1.3% vs. 7.5% at 300 °C, 1 bar), and much closer conversions at high temperatures (4.1% for Cu/Zn@C-mm vs. 5.0% for Cu/Zn@C-submm at 500 °C, 1 bar). Low temperatures further slowing down intra-pellet diffusion inside large pellets.

Catalyst molding after catalyst preparation, which is the processing of catalysts to suitable pellet size (0.2-0.4 mm) for bed packing, is a necessary step to allow efficient mass transport. The control of the sizes of the crystals for pyrolysis by crystal engineering provides an alternative way for catalyst molding for these MOF-derived catalysts. This method of tuning crystal sizes avoids the use of adhesives that are frequently employed to shape carbon-based catalysts into the appropriate pellet size. Direct pyrolysis of crystals creates a hierarchical catalyst assembly with small active Cu/Zn NPs of *nano*scale embedded in porous carbon matrix of *sub-millimeter* scale.

References

1 B. Jee, K. Eisinger, F. Gul-E-Noor, M. Bertmer, M. Hartmann, D. Himsl and A. Pöppl, *J. Phys. Chem. C*, 2010, **114**, 16630-16639.

2 M. K. Bhunia, J. T. Hughes, J. C. Fettinger and A. Navrotsky, *Langmuir*, 2013, **29**, 8140-8145.

3 T. M. Tovar, J. Zhao, W. T. Nunn, H. F. Barton, G. W. Peterson, G. N. Parsons and M. D. LeVan, *J. Am. Chem. Soc.*, 2016, **138**, 11449-11452.

4 O. Arbeláez, A. Orrego, F. Bustamante and A. L. Villa, *Top. Catal.*, 2012, **55**, 668-672.

5 I. Ud Din, M. S. Shaharun, D. Subbarao and A. Naeem, *J. Power Sources*, 2015, **274**, 619-628.

6 D. Wang, J. Zhao, H. Song and L. Chou, *Journal of Natural Gas Chemistry*, 2011, **20**, 629-634.

7 X. Zhang, X. Zhu, L. Lin, S. Yao, M. Zhang, X. Liu, X. Wang, Y.-W. Li, C. Shi and D. Ma, *ACS Catal.*, 2017, **7**, 912-918.

8 C. S. Chen, W. H. Cheng and S. S. Lin, *Appl. Catal. A- Gen.*, 2003, **238**, 55-67.

9 M. D. Porosoff, X. Yang, J. A. Boscoboinik and J. G. Chen, *Angew. Chem. Int. Ed.*, 2014, **53**, 6705-6709.

10 K. Kitamura Bando, K. Soga, K. Kunimori and H. Arakawa, *Appl. Catal., A*, 1998, **175**, 67-81.

11 Y. Hartadi, D. Widmann and R. J. Behm, *J. Catal.*, 2016, **333**, 238-250.